American Mineralogist, Volume 76, pages 218–229, 1991

Petrology and mineral chemistry of the Ascutney Mountain igneous complex

JILL S. SCHNEIDERMAN*
Department of Earth and Planetary Sciences, Harvard University, 24 Oxford Street, Cambridge, Massachusetts 02138, U.S.A.

ABSTRACT

The Ascutney Mountain igneous complex in southeastern Vermont is a Cretaceous member of the White Mountain plutonic-volcanic series. A subvolcanic complex, it consists of three stocks: gabbro-diorite, quartz syenite, and granite. A syenite porphyry ring dike rims a portion of the complex and contains large xenoliths of a unique breccia.

The gabbro-diorite consists of zoned plagioclase, augite, ferroan to magnesian hornblende, phlogopite, orthoclase, and quartz. A variety of syenites occur and consist of perthite (± albite ± orthoclase), ferro-edenite, annite, quartz, Fe-rich augite, and fayalite. The granite consists of microperthite, orthoclase, albite, phlogopite, and edenite. Magnetite, ilmenite, apatite, titanite, and zircon are common accessory minerals.

The temperature of the syenite magma was 890–1000 °C, and f_{O_2} ranged from $10^{-13.7}$ to $10^{-12.9}$ bars, as determined from the assemblage quartz + magnetite + ilmenite + fayalite. Pressure is constrained to have been approximately 2 kbar. Biotite equilibria indicate that f_{H_2O} of the syenite magma was 3300–4800 bars (a_{H_2O} = 1.8–2.8).

INTRODUCTION

The Ascutney Mountain igneous complex belongs to the White Mountain plutonic-volcanic series, a group of Mesozoic calc-alkalic to alkalic igneous complexes that occur in New Hampshire, southern Maine, and Vermont (Billings, 1928, 1943, 1956; Foland and Faul, 1977; McHone and Butler, 1984; Eby, 1987; Foland et al., 1985, 1988). Extensions of this series to the northwest and southeast, respectively, are the Monteregian Hills in the St. Lawrence Lowlands of Quebec and the New England Seamount Chain. (Eby, 1985; Gold, 1967; Philpotts, 1974; Fletcher et al., 1974; Bedard, 1988).

Ascutney Mountain is a classic locality for igneous petrology. It was as a result of his study of petrology and intrusive relations of the stocks there that Reginald Daly (1903) developed a theory of magmatic stoping as a mechanism for emplacement of large magma bodies. Subsequent work has focused on other mechanisms of intrusion (Chapman and Chapman, 1940), the Ascutney contact aureole (Nielson, 1973), the age of the rocks of the complex (Foland and Faul, 1977), and the isotopic composition of the constituent gabbro-diorite and granite (Foland et al., 1985, 1988). This paper reports on a field and petrologic study whose main purpose was to determine the physical conditions at the time of formation of the Ascutney complex. It is the first modern mineralogic and petrologic study of this classic field locality. Many of the igneous rocks and constituent minerals analyzed by electron microprobe in this study were collected and examined by R. A. Daly in his original investigation of Ascutney Mountain.

The Ascutney complex is located just west of the Connecticut River in southeastern Vermont (Fig. 1). Approximately 8 km (east-west) by 4 km (north-south) in size, the stocks and dikes of the complex were emplaced into Precambrian basement gneisses of the Chester dome and the overlying east-dipping Paleozoic metasediments. Superimposed on the regional metamorphic isograds is a well-developed contact metamorphic aureole around the main syenite stock (Nielson, 1973).

Radiometric ages obtained using the K-Ar method with biotite from intrusive rocks at Ascutney indicates that all the igneous rocks were emplaced in a short interval at 122 m.y. ± 1.2 m.y. (Foland and Faul, 1977; Foland et al., 1985). Other White Mountain plutonic-volcanic series rocks were emplaced at three time periods, ~225 m.y., 180 m.y., and 120 m.y., with the majority occurring around 180 m.y. The origin of this series cannot be attributed to the westward movement of the North American plate over a single, fixed mantle hot spot because there is no linear correlation between geographic position and age for the White Mountain, Monteregian, and New England Seamount intrusions (Foland and Faul, 1977; Vink et al., 1985). Rather, the emplacement is attributed to intrusion along transform faults or fracture zones of a failed Mesozoic rift (Ballard and Uchupi, 1975).

ROCK TYPES AND PETROGRAPHY

The Ascutney Mountain complex consists of three stocks which are, in order of decreasing age, gabbro-diorite, syenite, and granite as well as a partial ring dike and numerous discordant dikes (Fig. 2).

* Present address: Geology Department, Seaver Laboratory South, Pomona College, Claremont, California 91711, U.S.A.

0003–004X/91/0102–0218$02.00

Gabbro-diorite

The gabbro-diorite stock along the westernmost extent of the intrusive complex forms the main mass of Little Ascutney Mountain. It consists of gabbro and diorite with varied amounts of augite, hornblende, and biotite.

Plagioclase, alkali feldspar, and quartz are the other major minerals of the mafic intrusion, in addition to augite, biotite, and hornblende. Zircon, titanite, apatite, magnetite, and ilmenite are accessory minerals. The rocks are coarse to medium grained. Hornblende occurs as rims around augite and also displays resorbed edges. Inclusions of almost all minerals are observed in euhedral biotite grains. The order of crystallization was: apatite, titanite, zircon, magnetite, ilmenite, plagioclase, pyroxene, hornblende, biotite, alkali feldspar, quartz. In the field, the presence of gabbro inclusions in diorite indicates the earlier emplacement of the gabbro.

Syenite

Syenite composes the main mass of Ascutney Mountain and forms a crescentic ring dike on the south side of Little Ascutney Mountain. Daly (1903) described the main stock as a composite of four rock types: hornblende-biotite nordmarkite (quartz-bearing alkali syenite), porphyritic hornblende-biotite-augite nordmarkite, alkaline granite, and monzonite.

The syenite is composed of porphyritic, seriate, or subhedral granular medium-grained aggregates of perthite, hornblende, and biotite. Minor constituents include quartz, augite, and fayalite. Apatite, zircon, titanite, monazite, ilmenite, and magnetite are accessory minerals. Unlike its occurrence in the gabbro-diorite, hornblende in the syenite appears to have crystallized later than biotite because biotite inclusions occur in euhedral hornblende crystals. The syenite dike of Little Ascutney Mountain is structurally and chemically different from the syenites of the main mountain; it is fine grained, porphyritic, and less Fe-rich than those on Ascutney Mountain proper.

A variety of xenoliths occurs within the syenite stock. Cognate xenoliths of gabbro and diorite are present in the syenite and are direct field evidence for the older age of emplacement of the mafic stock. Other small mafic inclusions abundant in the syenite consist of fine-grained plagioclase, hornblende, biotite, and quartz. Foland et al. (1985) suggest that these inclusions were stoped from overlying cogenetic volcanic rock as the magma was emplaced. Volcanic rock occurs as a screen in the western portion of the syenite stock and as smaller elliptical bodies north of the northern summit of Ascutney Mountain. Large country rock xenoliths also occur. Breccia xenoliths abundant in the syenite porphyry dike of Little Ascutney Mountain were the subject of a detailed study by the author (Schneiderman, 1989). It is the presence of such xenoliths in the syenite at Ascutney, particularly at Crystal Cascade, that led Daly (1903) to formulate his theory of magmatic stoping as a mechanism for the emplacement of intrusive bodies.

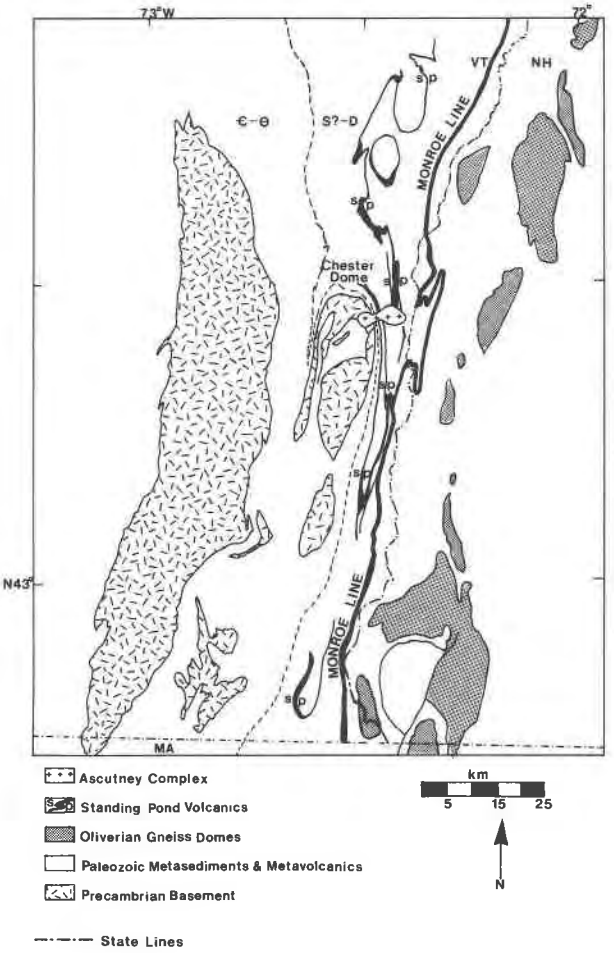

Fig. 1. Generalized geologic map of southeastern Vermont and southwestern New Hampshire showing location of the Ascutney igneous complex. Modified from Billings (1956), Doll et al. (1961), and Downie (1982).

Granite

Granite intrudes the southeast portion of the main syenite stock at Ascutney. It is medium to coarse grained and subhedral granular to subporphyritic. Microperthite, orthoclase, albite, quartz, and biotite are the major constituents. Hornblende is only rarely observed. Apatite, zircon, titanite, magnetite, and ilmenite are accessory minerals. Rare hornblende displays resorbed edges and biotite occurs as large, euhedral grains. This biotite granite is comparable to the Conway granite of the White Mountain plutonic-volcanic series in New Hampshire.

Dike rocks

Daly (1903) mapped four types of dike rocks at Ascutney Mountain: windsorite, paisanite, muscovite aplite, and lamprophyres. Balk and Krieger (1936) recognized devitrified felsites containing spherulites.

Daly (1903) defined the rock type windsorite to describe a leucocratic variety of quartz monzonite found near Windsor, Vermont. The rock type is characterized

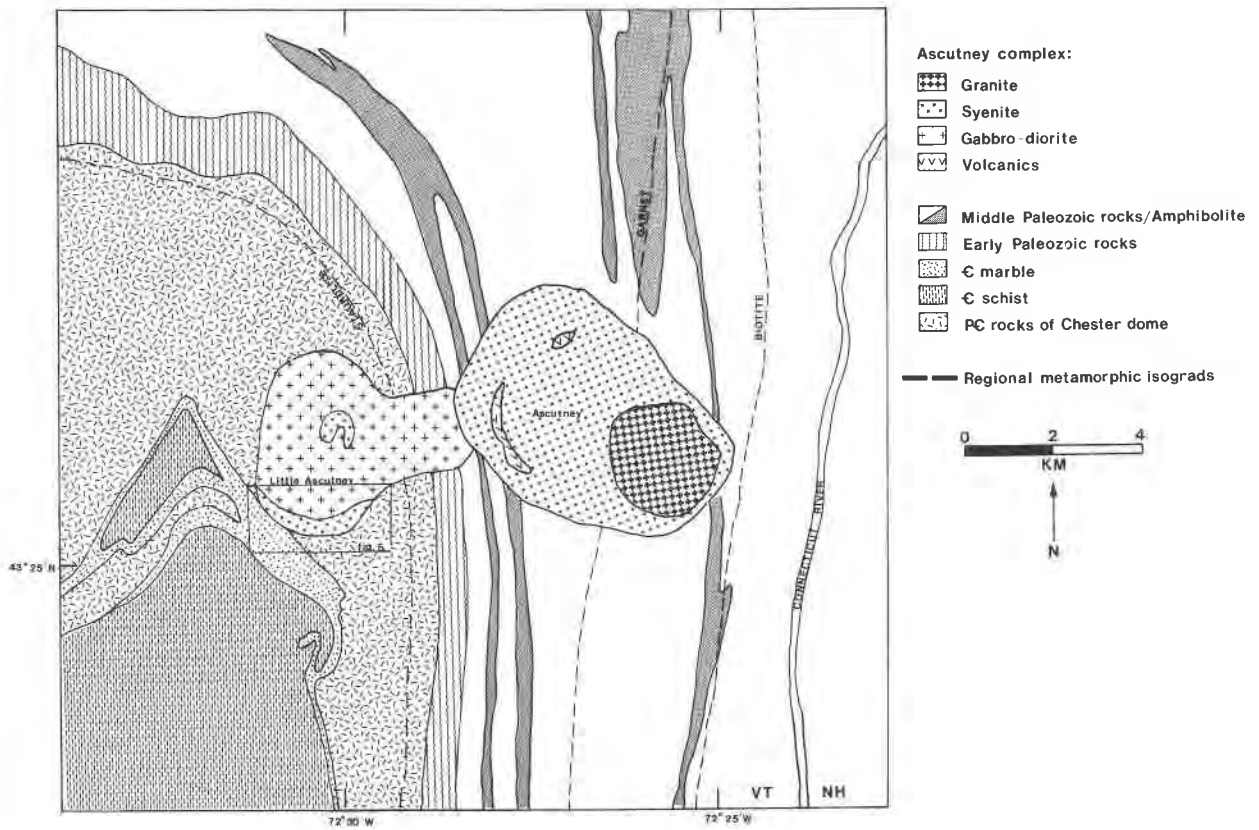

Fig. 2. Generalized geologic map of the Ascutney igneous complex. Modified from Daly (1903), Chapman and Chapman (1940), and Nielson (1973).

by high alkali content (K > Na), low Ca, Fe, and Mg (Daly, 1903). Two such dikes cut the eastern portion of the gabbro-diorite stock. They consist of plagioclase (oligoclase to andesine), orthoclase, microperthite, and biotite. Some of the plagioclase is rimmed by alkali feldspar. Quartz occurs interstitially and augite and hornblende are present though rare.

Fine-grained porphyritic dikes consisting of microperthite, orthoclase, quartz, and alkali-rich hornblende (paisanite) cut the gabbro-diorite, syenite ring dike, and the main syenite stock. Petrographically they resemble fine-grained phases of the main syenite stock. Like the syenite stock they contain abundant glomeroporphyritic aggregates of hornblende and biotite.

Muscovite aplite cuts the main syenite stock. It consists of quartz, orthoclase, albite, microperthite, and muscovite. Miarolitic cavities are common and contain terminated quartz crystals and books of muscovite.

Two other types of dikes, camptonite and diabase, cut the gabbro-diorite, syenite stock, and the country rock. The camptonite dikes are dark colored and fine grained and consist of plagioclase and hornblende that is altered to chlorite, epidote, calcite, and quartz. The diabase dikes, like those observed throughout the Connecticut River Valley, consist primarily of plagioclase and interstitial augite. Pyrite and magnetite are the main accessory minerals.

Aphanitic, felsite dikes studied by Balk and Krieger (1936) cut country rock gneisses, gabbro-diorite, and

Table 1. Representative pyroxene analyses

	Gabbro-diorite		Syenite	
	5237-7	21361-5	2187-7	AS84113-4
SiO_2	52.88	52.33	50.61	47.66
TiO_2	0.26	0.21	0.41	1.71
Al_2O_3	0.88	0.93	2.78	5.46
Cr_2O_3	0.00	0.01	0.02	0.04
MgO	14.17	13.89	9.91	12.03
FeO	9.68	9.70	20.56	11.15
MnO	0.61	0.47	0.65	0.38
CaO	21.10	21.44	11.44	19.16
Na_2O	0.42	0.36	1.08	1.01
Total	100.00	99.34	97.46	98.60
	Normalized to four cations			
Si	1.97	1.97	2.00	1.81
Ti	0.01	0.01	0.01	0.05
Al	0.04	0.04	0.13	0.24
Cr	0.00	0.00	0.00	0.00
Mg	0.79	0.78	0.59	0.68
Fe	0.30	0.31	0.68	0.35
Mn	0.02	0.02	0.02	0.01
Ca	0.84	0.86	0.49	0.78
Na	0.03	0.03	0.08	0.07

TABLE 2. Representative olivine analyses

	Syenite	
	5234-8	5234-9
SiO_2	30.87	30.85
TiO_2	0.02	0.03
Al_2O_3	0.00	0.00
Cr_2O_3	0.03	0.04
MgO	1.78	1.76
FeO	64.28	63.58
MnO	4.11	4.42
NiO	0.03	0.03
CaO	0.10	0.12
Total	101.22	100.83
Normalized to three cations		
Si	1.02	1.02
Ti	0.00	0.00
Al	0.00	0.00
Cr	0.00	0.00
Mg	0.09	0.09
Fe	1.77	1.76
Mn	0.12	0.12
Ni	0.00	0.00
Ca	0.00	0.00

quartz syenite of Little Ascutney. They are distinguished by flow-banding, spherulites, and a devitrified groundmass. The spherulites occur in clusters that are roughly parallel to the flow-banding and are composed of microlites arranged in a radial fashion.

Mineral compositions

Mineral compositions were determined with an automated three spectrometer Cameca MBX electron microprobe at Harvard University. The data reported in this study represent complete microprobe analyses for up to 14 elements: Si, Al, Ti, Fe, Mg, Mn, Zn, Cr, Ca, Ba, K, Na, F, Cl. The spectrometers were prioritized to measure Na, K, F, and Cl first during the analysis of biotite and amphibole. Oxide weight percents were converted from X-ray intensities using the procedures of Bence and Albee (1968) and the correction factors modified from Albee and Ray (1970). Operating conditions were 15 kV accelerating potential and 15 nA beam current. A set of simple oxides and silicates was used for primary standards. Counting statistics were set for 1% standard deviation.

For exsolved feldspars, bulk compositions were obtained for cryptoperthite with regular 1–2 μm exsolution lamellae by systematic analysis with a 16 μm × 16 μm raster beam over 20–25 microprobe areas per grain. Compositions of lamellae and host were determined for microperthite (5–7 μm lamellae) grains using a 1–2 μm point beam.

Note that, in the tables of representative mineral analyses, the amalgam of numbers and letters that precedes a hyphen, if present, is the rock sample number; the number after the hyphen is the number of the analysis. Therefore, for example, the minerals for which analyses were obtained, fayalite analysis 5234-8, plagioclase 5234-5, alkali feldspar 5234-5, and Fe-Ti oxides 5234-7, all come from the same rock sample.

Pyroxene

Clinopyroxene is abundant in the gabbro-diorite of Little Ascutney Mountain and sometimes constitutes as much as 20% of the rock. It is a minor mineral phase in the syenite, subordinate to biotite and hornblende, and is not found in the granite. It is colorless to pale greenish brown, lacks pleochroism, and is simply twinned. Representative electron microprobe analyses are given in Table 1.

TABLE 3. Representative plagioclase analyses

	Gabbro-diorite				Syenite			Granite			
	Core 21361	Rim 21361	Core 3480	Rim 3480	5234-5	AS841A-8	AS84113-1	Core 21369	Rim 21369	Core 5239	Rim 5239
SiO_2	48.20	57.61	47.83	59.08	61.13	65.34	66.44	62.34	66.37	65.90	66.22
Al_2O_3	32.63	26.40	32.98	25.53	24.53	21.19	20.96	22.91	20.61	20.98	20.79
TiO_2	0.09	0.06	0.04	0.01	0.05	0.00	0.03	0.05	0.01	0.04	0.03
FeO	0.35	0.24	0.39	0.23	0.14	0.27	0.14	0.20	0.21	0.18	0.16
MgO	0.01	0.00	0.01	0.01	0.00	0.01	0.00	0.02	0.02	0.01	0.00
BaO	0.02	0.04	0.01	0.01	0.13	0.03	0.00	0.09	0.00	0.01	0.01
SrO	0.16	0.15	0.20	0.17	0.11	0.07	0.01	0.19	0.03	0.09	0.06
CaO	15.78	8.30	16.04	7.01	5.72	2.21	1.66	4.32	1.51	1.88	1.54
Na_2O	2.47	6.56	2.27	7.15	8.26	9.46	10.66	8.46	10.35	10.23	10.38
K_2O	0.08	0.31	0.08	0.55	0.36	1.37	0.40	0.67	0.48	0.58	0.42
Total	99.79	99.67	99.85	99.70	100.43	99.95	100.30	99.35	99.59	99.90	99.61
Atomic proportions calculated on the basis of eight O atoms											
Si	2.22	2.59	2.20	2.65	2.71	2.89	2.91	2.79	2.93	2.91	2.92
Al	1.77	1.40	1.79	1.35	1.28	1.11	1.08	1.21	1.07	1.09	1.08
Ti	0.00	0.00	0.00	0.00	0.00	0.00	0.00	0.00	0.00	0.00	0.00
Fe	0.01	0.01	0.02	0.01	0.01	0.01	0.01	0.01	0.01	0.01	0.01
Mg	0.00	0.00	0.00	0.00	0.00	0.00	0.00	0.00	0.00	0.00	0.00
Ba	0.00	0.00	0.00	0.00	0.00	0.00	0.00	0.00	0.00	0.00	0.00
Sr	0.00	0.00	0.01	0.00	0.00	0.00	0.00	0.01	0.00	0.00	0.00
Ca	0.78	0.40	0.79	0.34	0.27	0.11	0.08	0.21	0.07	0.09	0.07
Na	0.22	0.57	0.20	0.62	0.71	0.81	0.91	0.73	0.89	0.87	0.89
K	0.01	0.02	0.01	0.03	0.02	0.08	0.02	0.04	0.03	0.03	0.02
Σ cation	5.01	5.00	5.01	5.00	5.00	5.01	5.01	4.99	4.99	5.00	5.00

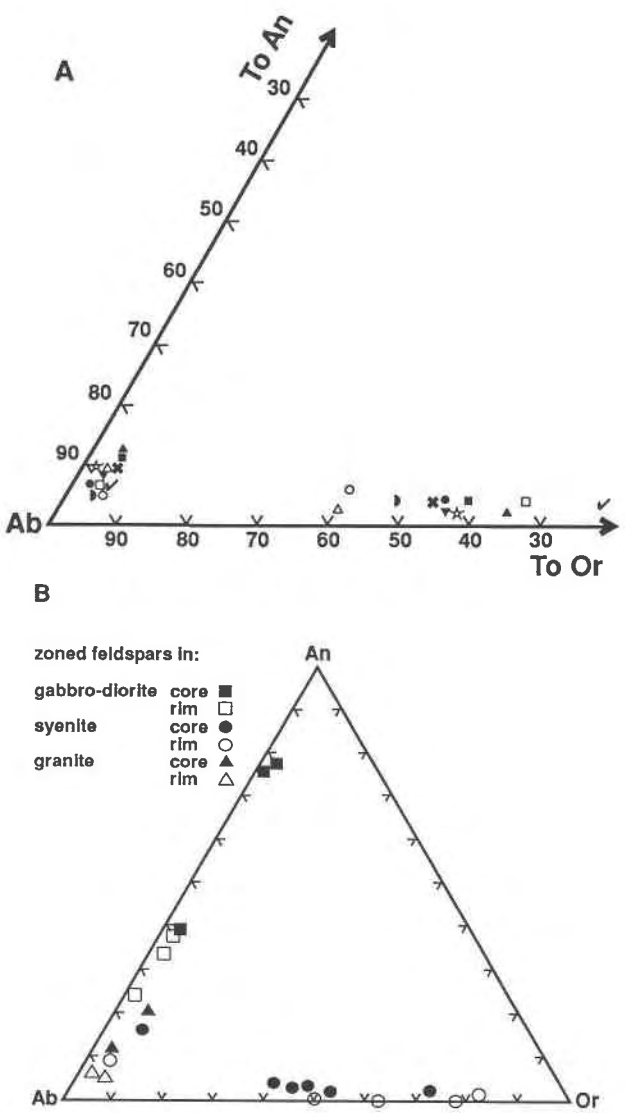

Fig. 3. Ternary projection of feldspar compositions from gabbro-diorite, syenite, and granite from Ascutney, Vermont. (**A**) Compositions of coexisting unzoned plagioclase and unzoned alkali-feldspars. Triangle symbols represent coexisting feldspars from granite. Other symbols represent coexisting feldspars from syenite. (**B**) Core and rim compositions for zoned plagioclase and alkali feldspar grains and compositions of coexisting plagioclase rims and alkali feldspar rims.

Fayalite

Fayalite occurs as an accessory mineral in the syenite. Representative electron microprobe analyses (Table 2) show that its composition is $Fa_{89}Fo_5Te_6$. It is commonly rimmed by amphibole and biotite and is usually altered to iddingsite.

Feldspars

Both plagioclase and alkali feldspar occur in all the intrusive rocks of the Ascutney complex. Plagioclase is the predominant feldspar in the gabbro-diorite. The syenite is hypersolvus although discrete grains of potassium feldspar and albite are observed occasionally. In the granite, plagioclase and potassic feldspar occur in subequal proportions. The feldspars occur as subhedral laths and anhedral grains ranging in size from 0.5 mm to 4 mm. Plagioclase is twinned according to albite and Carlsbad twin laws. Myrmekitic intergrowths of wormy quartz in plagioclase are observed between plagioclase and potassium feldspar in the gabbro-diorite.

In the gabbro-diorite and granite, plagioclase is normally zoned with cores of X_{An} = 0.40–0.50 and X_{An} = 0.10–0.15 and rims of X_{An} = 0.20 and X_{An} = 0.0–0.50, respectively (Table 3). In the syenite, small, twinned grains of albite (X_{An} = 0.0–0.10) are mantled by potassic feldspar. K content of plagioclase cores is highest in syenite (6 wt%). Unzoned plagioclase in the syenite is X_{An} = 0.08 and that in the granite is X_{An} = 0.10 (Fig. 3a).

Alkali feldspar is present as crypto- and microperthite, orthoclase, and microcline. Both the perthite and orthoclase have Carlsbad twinning and the microcline displays characteristic grid twinning. Small unzoned alkali feldspar grains range in composition from X_{Or} = 0.40 to X_{Or} = 0.79 (Fig. 3a). Large alkali feldspars are normally zoned from sodic cores to potassic rims (Fig. 3b). Cores of many perthite grains are weathered and altered to fine-grained sericite. Granophyric and micrographic intergrowths of quartz in perthite are common. Representative electron microprobe analyses and structural formulae are given in Table 4.

Amphibole

Amphibole in all intrusive rocks of the Ascutney complex is strongly pleochroic from light greenish brown to gray olive-green, displays well developed cleavage, and is frequently twinned parallel to (100). It frequently rims augite and contains inclusions of ilmenite, magnetite, zircon, and apatite.

Amphiboles from Ascutney intrusions are calcic: $^{M4}(Ca + Na) \geq 1.34$; $^{M4}Na < 0.67$ (Leake, 1978). In the syenite, amphibole is ferro-edenite and ferro-edenitic hornblende; the granite contains edenite; in contrast, the gabbro-diorite and the porphyritic syenite at Little Ascutney have ferro-hornblende and magnesio-hornblende (Table 5). Compositional variations within amphibole are as follows: wt% Al_2O_3 correlates inversely with SiO_2 whereas it correlates positively with Na_2O, K_2O, and TiO_2, indicating coupled substitutions.

Figure 4 shows cationic Mg/(Mg + Fe^{2+} + Mn) vs. $^{[6]}Al/^{[4]}Al$ of the Ascutney amphiboles. Amphiboles in the gabbro-diorite and granite are relatively enriched in Mg compared to other amphiboles in the complex. An inverse correlation between Mg and $^{[4]}Al$ of amphibole in syenite indicates a tschermak substitution.

Bedard (1988) showed that Monteregian Hills and White Mountain series amphiboles plot in distinct fields with regard to Ca + $^{[4]}Al$ and Si + Na + K. Ascutney amphiboles fall within Bedard's field of White Mountain series amphiboles indicating that the gabbro-diorite, syenite, and granite crystallized from silica-saturated magmas.

Table 4. Representative alkali feldspar analyses

	Gabbro-diorite	Syenite									Granite	
					AS-84-10		AS848-13					
	3480-7	3501-10	5234-5	AS841A-8	Core	Rim	Host core	Host rim	Lamellae core	Lamellae rim	21369	5239-7
SiO_2	64.56	65.93	65.47	65.55	65.28	65.36	65.17	65.34	67.47	67.58	65.83	65.09
Al_2O_3	18.34	18.95	19.43	18.76	18.72	18.67	18.57	18.53	19.98	19.88	18.83	18.46
TiO_2	0.02	0.01	0.01	0.01	0.00	0.00	0.00	0.00	0.00	0.00	0.06	0.05
FeO	0.12	0.19	0.27	0.22	0.06	0.06	0.05	0.05	0.07	0.05	0.16	0.16
MgO	0.00	0.03	0.00	0.01	0.00	0.00	0.00	0.00	0.00	0.00	0.00	0.01
BaO	0.40	0.05	0.07	0.13	0.07	0.05	0.04	0.07	0.00	0.01	0.12	0.17
SrO	0.16	0.01	0.03	0.06	0.02	0.03	0.04	0.06	0.02	0.03	0.02	0.08
CaO	0.06	0.20	0.71	0.26	0.13	0.08	0.05	0.02	0.53	0.50	0.25	0.12
Na_2O	1.52	4.52	4.76	3.26	3.03	2.37	1.32	1.40	10.39	9.95	5.52	2.92
K_2O	13.61	10.08	9.11	11.50	12.16	13.15	14.58	14.55	1.50	2.21	8.07	11.57
Total	98.79	99.97	99.86	99.76	99.47	99.77	99.82	100.02	99.96	100.21	98.86	98.63
Atomic proportions calculated on the basis of eight O atoms												
Si	3.00	2.99	2.96	2.99	2.99	3.00	3.00	3.00	2.97	2.97	2.99	3.00
Al	1.01	1.01	1.04	1.01	1.01	1.01	1.01	1.00	1.04	1.03	1.01	1.00
Ti	0.00	0.00	0.00	0.00	0.00	0.00	0.00	0.00	0.00	0.00	0.00	0.00
Fe	0.01	0.01	0.01	0.01	0.00	0.00	0.00	0.00	0.00	0.00	0.01	0.01
Mg	0.00	0.00	0.00	0.00	0.00	0.00	0.00	0.00	0.00	0.00	0.00	0.00
Ba	0.01	0.00	0.00	0.00	0.00	0.00	0.00	0.00	0.00	0.00	0.00	0.00
Sr	0.00	0.00	0.00	0.00	0.00	0.00	0.00	0.00	0.00	0.00	0.00	0.00
Ca	0.00	0.01	0.03	0.01	0.01	0.00	0.00	0.00	0.03	0.02	0.01	0.01
Na	0.14	0.40	0.42	0.29	0.27	0.21	0.12	0.13	0.89	0.85	0.49	0.26
K	0.81	0.58	0.53	0.67	0.71	0.77	0.86	0.85	0.08	0.12	0.47	0.68
Σ cation	4.97	5.00	4.99	4.98	4.99	4.99	4.99	4.99	5.00	5.00	4.98	4.97

Biotite

Biotite occurs in all intrusive rocks of the Ascutney complex in glomeroporphyritic aggregates with amphibole, augite, ilmenite, magnetite, zircon, and apatite. It is strongly pleochroic. Also, well-developed pleochroic haloes surround zircon inclusions. In the gabbro-diorite and granite biotite is subhedral, whereas in the syenite, it forms irregularly shaped grains and occurs as inclusions in hornblende, indicating its early crystallization.

Biotite structural formulae were calculated on the basis of 11 O atoms since high valence cations substitute for divalent ones in Ascutney biotite and result in octahedral vacancies (Table 6).

Biotite from gabbro-diorite and granite has $Fe/(Fe^{2+} + Mg)$ between 0.41 and 0.45, biotite from the syenite ring dike ranges from 0.50 to 0.72, and biotite from the syenite stock is most Fe rich, $Fe/(Fe^{2+} + Mg) = 0.62$ to 0.85. Biotite from all rock types has low Al but high K and F contents.

The biotite compositions reflect both tschermak and octahedral vacancy substitutions. The positive correlation between $^{[4]}Al$ and Ti indicates a component of titanium tschermak substitution. Also, an apparent correlation between higher Ti contents and lower octahedral site occupancies suggests the coupling of Ti substitutions with an octahedral vacancy ($2R^{2+} = R^{4+} + \square$).

Fe-Ti oxides

Magnetite and ilmenite occur in all intrusive rocks of the complex. They occur in subequal proportions of the gabbro-diorite and granite, but ilmenite is more abundant than magnetite in the syenite. Both minerals occur as discrete, subhedral to anhedral grains distributed equally throughout the rock, in glomeroporphyritic aggregates, or as inclusions in augite, hornblende, and biotite. Magnetite flakes form rims around biotite adjacent to alkali feldspar, a texture that may result from the reaction annite + ilmenite = potassium feldspar + ulvospinel + H_2O (Diamond and Frost, 1988). Table 7 shows representative microprobe analyses of coexisting oxides.

Geobarometry and Geothermometry

Pressure

Andalusite in the Ascutney contact aureole indicates that pressure during emplacement of the intrusive complex was no greater than 3.8 kbar (Holdaway, 1971; Nielson, 1973; Schneiderman, 1987). Compositions and textures of the mafic silicates in the syenite supply lower pressure estimates.

Annite and quartz rim fayalite which is adjacent to potassium feldspar (Fig. 5). Assuming that the melting curve of the Ascutney quartz syenite is comparable to the granite minimum melting curve, the intersection of this curve with the stability curve for the reaction

$$\underset{\text{annite}}{2KFe_3AlSi_3O_{10}(OH)_2} + \underset{\text{quartz}}{3SiO_2} = \underset{\text{potassium feldspar}}{2KAlSi_3O_8} + \underset{\text{fayalite}}{3Fe_2SiO_4} + \underset{\text{vapor}}{2H_2O}$$

indicates a pressure of at least 1.5 kbar at the time of intrusion (Fig. 6). Although Ca and Na in the A-site and octahedral Al decrease the stability of annite (Wones and Eugster, 1965) they are not substantial components of the Ascutney biotite. However, Mg, Ti, and F, all present in Ascutney biotite, expand the *P-T* field of Fe-rich biotite (Rutherford, 1969; Eugster and Wones, 1962).

TABLE 5. Representative amphibole analyses

	Gabbro-diorite			Syenite					Granite		
	21361-1	3480-2	5237-3	AS848-4	AS8444-7	3490-2	2187-4	5250-4A	21369-1	21369-2A	21369-2E
SiO_2	41.87	47.14	48.01	43.14	46.64	46.44	41.80	42.56	48.03	48.04	47.77
Al_2O_3	10.90	6.12	6.15	7.57	5.44	5.35	8.00	7.13	5.40	5.46	5.38
TiO_2	4.35	1.23	0.99	0.29	0.20	0.86	1.60	1.58	0.81	1.15	1.05
FeO*	13.01	14.18	13.83	27.99	23.43	22.54	29.03	27.18	14.47	38.88	14.46
MgO	12.57	13.72	14.19	4.22	7.59	8.22	3.66	4.88	13.67	13.85	13.55
MnO	0.27	0.34	0.49	1.27	0.99	1.08	0.98	0.94	1.18	1.05	1.17
ZnO	0.01	0.01	0.04	0.05	0.06	0.06	0.06	0.08	0.04	0.02	0.04
Cr_2O_3	0.02	0.01	0.00	0.00	0.01	0.00	0.02	0.01	0.01	0.03	0.01
CaO	11.31	11.71	10.77	10.33	11.68	10.56	10.27	9.90	10.99	10.96	11.05
BaO	0.14	0.03	0.03	0.02	0.02	0.01	0.02	0.03	0.03	0.02	0.00
Na_2O	2.35	1.03	1.28	1.91	1.28	1.58	2.21	2.18	2.17	2.26	2.23
K_2O	1.04	0.67	0.53	0.97	0.70	0.71	1.24	1.09	0.79	0.72	0.74
F	0.20	0.22	0.22	0.66	0.64	0.70	0.92	1.15	1.62	1.64	1.52
Cl	0.03	0.15	0.11	0.42	0.18	0.20	0.53	0.35	0.07	0.10	0.10
O = F + Cl	−0.09	−0.13	−0.12	−0.37	−0.31	−0.34	−0.51	−0.56	−0.70	−0.71	−0.66
Total	97.98	96.43	96.52	98.49	98.54	97.97	99.83	98.50	98.58	98.47	98.41
Atomic proportions calculated on the basis of 13 cations excluding Ca, Na, Ba, K											
Si	6.20	6.97	7.00	6.75	7.13	7.07	6.54	6.66			
$^{[4]}Al$	1.80	1.03	1.00	1.25	0.98	0.94	1.46	1.32	7.05	7.06	7.04
Σ T-site	8.00	8.00	8.00	8.00	8.01	8.01	8.00	7.98	0.94	0.94	0.93
$^{[6]}Al$	0.10	0.04	0.06	0.14	0.11	0.02	0.02	0.00	0.00	0.01	0.00
Ti	0.48	0.14	0.11	0.03	0.02	0.10	0.19	0.19	0.09	0.13	0.12
Fe^{3+}**	0.27	0.58	0.90	0.81	0.36	0.67	0.70	0.78	0.55	0.46	0.49
Cr^{3+}	0.00	0.00	0.00	0.00	0.00	0.00	0.00	0.00	0.00	0.00	0.00
Mg	2.77	3.03	3.08	0.98	1.73	1.86	0.85	1.14	2.99	3.03	2.98
Fe^{2+}	1.34	1.18	0.79	2.86	2.64	2.20	3.10	2.78	1.23	1.25	1.29
Zn	0.00	0.00	0.00	0.01	0.01	0.01	0.01	0.01	0.00	0.00	0.00
Mn	0.03	0.04	0.06	0.17	0.13	0.14	0.13	0.10	0.14	0.12	0.12
Σ C-site	4.99	5.01	5.00	5.00	5.00	5.00	5.00	5.00	5.00	5.00	5.00
Mn	0.00	0.00	0.00	0.00	0.00	0.00	0.00	0.03	0.01	0.01	0.03
Ca	1.79	1.86	1.68	1.73	1.91	1.72	1.72	1.66	1.73	1.73	1.75
Na	0.21	0.14	0.32	0.27	0.09	0.28	0.28	0.31	0.26	0.26	0.22
Σ B-site	2.00	2.00	2.00	2.00	2.00	2.00	2.00	2.00	2.00	2.00	2.00
Na	0.46	0.15	0.05	0.31	0.29	0.18	0.39	0.35	0.36	0.38	0.42
K	0.20	0.13	0.10	0.19	0.14	0.14	0.25	0.22	0.15	0.14	0.14
Ba	0.01	0.00	0.00	0.00	0.00	0.00	0.00	0.00	0.00	0.00	0.00
Σ A-site	0.67	0.28	0.15	0.50	0.43	0.32	0.64	0.57	0.51	0.52	0.56
$100 \times XFe^{2+}$	32.60	28.03	20.41	74.48	60.41	54.19	78.48	70.92	29.15	29.21	30.21

* Total Fe measured as FeO.
** Fe^{3+} calculated by charge balance for 23 O atoms.

Compositions of amphibole in the syenite approach those of hastingsite. Near FMQ conditions, the stability curve for the reaction hastingsite = magnetite + hedenbergite$_{ss}$ + plagioclase + garnet$_{ss}$ + fluid intersects the granite minimum melting curve at ~2.3 kbar (Thomas, 1977, 1982). Substitutions of Mg, F, and K shift the stability curve to higher temperatures toward that of annite, indicating pressures less than 2.3 kbar (Cameron and Gibbs, 1973; Helz, 1979).

Biotite inclusions in hornblende indicate that the thermal stability of hornblende did not exceed that of the annite. In contrast, gabbro-diorite and granite contain biotite with hornblende inclusions. The inclusions are magnesiohastingsite which has a greater thermal stability than hastingsite (Semet and Ernst, 1981; Thomas, 1982).

Temperature

Temperatures ranging from 550 to 725 °C were determined for the syenite samples using the Stormer (1975) and Powell and Powell (1977) geothermometers. However, it seems likely that these temperatures only reflect temperatures of subsolidus recrystallization and reequilibration.

One syenite sample (5234) contained the assemblage quartz + fayalite + ilmenite + magnetite and thus it was possible to apply the QUIIF equilibrium technique of Frost et al. (1988) to estimate temperature of the syenite. Assuming 2 kbar pressure and $X_{ilm} = 0.97$, the calculated temperature of the syenite is 890–1000 °C. This temperature range is corroborated by the contact aureole assemblage cordierite + spinel + corundum + sillimanite. Also, fayalite-bearing rhyolites from other quartz-saturated igneous rocks show similarly high temperatures (Frost et al., 1988).

Oxygen fugacity

Coexisting oxides in the syenite occur as discrete grains. However, like the feldspars, the oxides have undergone reequilibration. Therefore, f_{O_2} could not be determined using the Fe-Ti oxide oxybarometer (Buddington and Lindsley, 1964; Spencer and Lindsley, 1981). It was possible, though, to use the QUIIF assemblage of syenite

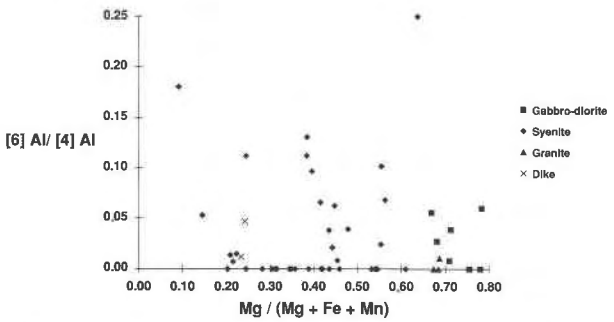

Fig. 4. Mg/(Mg + Fe^{2+} + Mn) vs. $^{[6]}Al/^{[4]}Al$ for amphiboles in Ascutney intrusions.

sample 5234 to estimate f_{O_2} (Frost et al., 1988). Once again, taking X_{ilm} = 0.97 and 2 kbar pressure, the f_{O_2} ranges from $10^{-13.7}$ bars to $10^{-12.9}$ bars, just below the FMQ buffer.

H_2O activity

The temperature and f_{O_2} estimates were used with the compositions of alkali feldspar, magnetite, and biotite, assuming ideal solution, to calculate f_{H_2O}. Modifying the equation of Wones (1981) to include the effects of F substitution for OH on the activity of annite (Czmanske and Wones, 1973) and using it with the estimated activities of annite in biotite (0.85), $KAlSi_3O_8$ in alkali feldspar (0.6), Fe_3O_4 in spinel (0.86), T = 890–1000 °C, and f_{O_2} = $10^{-13.7}$–$10^{-12.9}$ bars, syenite sample 5234 gives values of f_{H_2O} ranging from approximately 3300–4800 bars. [The crystal chemical models of Waldbaum and Thompson (1969) and Stormer (1983) were used to calculate the activities of $KAlSi_3O_8$ in feldspar and Fe_3O_4 in spinel, respectively.] This f_{H_2O} is considered to be a maximum because the biotite from Ascutney syenite most likely contains Fe^{3+} and the activity of annite in biotite would be less than 0.85. Using the tabulations of Burnham et al. (1969) and taking the pressure at the time of emplacement to be approximately 2 kbar as explained previously, the calculated H_2O activity ranges from 1.8–2.8. The range of values reflects the temperature range of 890–1000 °C. This high H_2O activity indicates that the magma was fluid saturated.

This is not a surprising result. Early crystallization of anhydrous minerals would contribute to increased a_{H_2O}

TABLE 6. Representative biotite analyses

	Gabbro-diorite			Syenite							Granite		
	3480-5	5237-4	21361-1	AS848-2	3490-5	21367-1	AS 841A-4	2187-1	5250-1	5234-4	5239-4	21369-3A	AS842A
SiO_2	36.09	36.11	36.40	33.79	34.63	34.87	35.44	34.89	34.97	35.01	38.83	38.23	38.93
Al_2O_3	13.59	13.55	13.47	12.81	13.14	12.92	12.47	11.97	11.75	11.83	11.46	12.17	11.83
TiO_2	4.66	4.94	4.88	3.71	4.21	6.07	4.21	3.32	2.52	4.02	1.92	3.17	2.26
FeO*	18.03	17.54	18.22	31.03	26.57	24.72	28.73	33.22	32.95	32.41	17.55	16.21	15.05
MgO	12.82	13.02	12.47	3.83	7.21	7.68	5.81	3.34	3.88	3.31	14.28	14.62	16.00
MnO	0.13	0.17	0.15	0.70	0.47	0.37	0.35	0.46	0.34	0.52	1.14	0.73	0.86
ZnO	0.01	0.02	0.03	0.11	0.08	0.07	0.18	0.08	0.07	0.16	0.09	0.03	0.06
Cr_2O_3	0.02	0.02	0.03	0.11	0.15	0.05	0.03	0.01	0.06	0.02	0.03	0.01	0.04
CaO	0.00	0.00	0.00	0.04	0.02	0.03	0.04	0.02	0.04	0.01	0.00	0.00	0.01
BaO	0.72	0.59	0.37	0.08	1.71	1.90	0.10	0.06	0.10	0.11	0.03	0.12	0.07
Na_2O	0.10	0.17	0.15	0.07	0.09	0.44	0.37	0.07	0.06	0.08	0.16	0.22	0.24
K_2O	9.53	9.60	9.60	9.11	8.85	8.46	8.68	9.19	9.20	9.28	9.86	9.79	10.04
F	0.39	0.35	0.31	0.70	0.94	0.96	1.69	1.04	0.96	1.04	3.04	2.61	3.56
Cl	0.27	0.23	0.14	0.49	0.36	0.15	0.58	0.83	1.10	0.57	0.05	0.09	0.13
Subtotal	96.36	96.31	96.22	96.58	98.43	98.69	98.68	98.50	98.00	98.37	98.44	98.00	99.08
O = F + Cl	−0.23	−0.20	−0.16	−0.41	−0.48	−0.44	−0.84	−0.63	−0.65	−0.57	−1.29	−1.12	−1.53
H_2O	3.60	3.63	3.66	3.15	3.18	3.24	2.75	2.92	2.88	2.99	2.43	2.63	2.21
Total	99.73	99.74	99.72	99.32	101.13	101.49	100.59	100.79	100.23	100.79	99.58	99.51	99.76
Atomic proportions calculated on the basis of 11 O atoms													
Si	2.76	2.75	2.77	2.77	2.74	2.72	2.82	2.84	2.87	2.84	2.96	2.90	2.93
$^{[4]}Al$	1.22	1.22	1.21	1.23	1.23	1.19	1.17	1.15	1.13	1.13	1.03	1.09	1.05
$^{[6]}Al$	0.00	0.00	0.00	0.01	0.00	0.00	0.00	0.00	0.01	0.00	0.00	0.00	0.00
Ti	0.23	0.28	0.28	0.23	0.25	0.36	0.25	0.20	0.16	0.25	0.11	0.18	0.13
Fe	1.15	1.12	1.16	2.13	1.76	1.61	1.91	2.26	2.26	2.20	1.12	1.03	0.95
Mn	0.01	0.01	0.01	0.05	0.03	0.02	0.02	0.03	0.02	0.04	0.07	0.05	0.06
Mg	1.46	1.48	1.42	0.47	0.85	0.89	0.69	0.41	0.47	0.40	1.62	1.65	1.80
Zn	0.00	0.00	0.00	0.01	0.01	0.00	0.01	0.01	0.00	0.01	0.01	0.00	0.00
Cr	0.00	0.00	0.00	0.01	0.01	0.00	0.00	0.00	0.00	0.00	0.00	0.00	0.00
Ca	0.00	0.00	0.00	0.00	0.00	0.00	0.00	0.00	0.00	0.00	0.00	0.00	0.00
Ba	0.02	0.02	0.01	0.00	0.05	0.06	0.00	0.00	0.00	0.00	0.00	0.00	0.00
Na	0.02	0.03	0.02	0.01	0.01	0.07	0.06	0.01	0.01	0.01	0.02	0.03	0.04
K	0.93	0.93	0.93	0.95	0.89	0.84	0.88	0.95	0.96	0.96	0.96	0.95	0.96
F	0.09	0.08	0.08	0.18	0.24	0.24	0.43	0.27	0.25	0.27	0.73	0.63	0.85
Cl	0.04	0.03	0.02	0.07	0.05	0.02	0.08	0.12	0.15	0.08	0.01	0.01	0.02
Σ oct. c	2.85	2.89	2.87	2.91	2.91	2.88	2.88	2.91	2.92	2.90	2.93	2.94	2.94
XFe	0.44	0.43	0.45	0.82	0.67	0.64	0.74	0.85	0.83	0.85	0.41	0.38	0.34

* Total Fe measured as FeO.

TABLE 7. Representative oxide analyses

	Gabbro-diorite		Syenite						Granite			
	5237 mag	5237 ilm	5234-7 mag	5234-7 ilm	5240 mag	5240 ilm	5250 mag	5250 ilm	AS-84-1A mag	AS-84-1A ilm	5239 mag	5239 ilm
SiO_2	0.08	0.02	0.10	0.03	0.10	0.07	0.10	0.09	0.13	0.06	0.06	0.06
TiO_2	0.31	46.30	4.43	49.01	0.62	48.44	5.10	48.97	5.51	48.98	0.26	56.18
Al_2O_3	0.46	0.03	0.47	0.02	0.16	0.04	0.69	0.08	0.68	0.04	0.08	0.04
V_2O_3	0.50	0.43	0.10	0.33	0.20	0.32	0.11	0.32	0.08	0.25	0.12	0.40
Cr_2O_3	0.13	0.05	0.04	0.02	0.08	0.03	0.07	0.00	0.00	0.01	0.04	0.04
Fe_2O_3	68.12	13.12	60.14	3.37	67.63	4.21	58.81	3.63	58.08	4.53	68.58	0.00
FeO	31.76	38.83	35.27	43.55	31.54	42.30	35.87	43.56	36.15	42.60	31.53	37.47
MnO	0.03	1.58	0.28	2.45	0.11	3.11	0.32	2.28	0.41	2.67	0.03	0.27
MgO	0.07	0.79	0.00	0.03	0.03	0.08	0.00	0.01	0.00	0.00	0.00	0.00
CaO	0.01	0.02	0.02	0.05	0.21	0.04	0.03	0.01	0.03	0.02	0.00	0.04
ZnO	0.12	0.00	0.05	0.02	0.03	0.05	0.20	0.08	0.29	0.16	0.02	0.04
NiO	0.00	0.19	0.04	1.88	0.01	1.89	0.01	1.65	0.01	1.25	0.03	1.94
Total	101.58	101.36	100.93	100.75	100.72	100.57	101.31	100.68	101.36	100.57	100.75	96.48
	Magnetite normalized to 3 cations; ilmenite normalized to 2 cations											
Si	0.00	0.00	0.00	0.00	0.00	0.00	0.00	0.00	0.01	0.00	0.00	0.00
Ti	0.01	0.87	0.13	0.93	0.02	0.92	0.15	0.93	0.16	0.93	0.01	0.12
Al	0.02	0.00	0.02	0.00	0.01	0.00	0.03	0.00	0.03	0.00	0.00	0.00
V	0.02	0.01	0.00	0.01	0.01	0.01	0.00	0.01	0.00	0.01	0.00	0.01
Cr	0.00	0.00	0.00	0.00	0.00	0.00	0.00	0.00	0.00	0.00	0.00	0.00
Fe^{3+}	1.94	0.25	1.71	0.06	1.94	0.08	1.67	0.07	1.65	0.09	1.97	0.00
Fe^{2+}	1.00	0.81	1.12	0.92	1.01	0.89	1.13	0.92	1.14	0.90	1.01	0.83
Mn	0.00	0.03	0.01	0.05	0.00	0.07	0.01	0.05	0.01	0.06	0.00	0.01
Mg	0.00	0.03	0.00	0.00	0.00	0.00	0.00	0.00	0.00	0.00	0.00	0.00
Ca	0.00	0.00	0.00	0.00	0.01	0.00	0.00	0.00	0.00	0.00	0.00	0.00
Zn	0.00	0.00	0.00	0.00	0.00	0.00	0.01	0.00	0.01	0.00	0.00	0.00
Ni	0.00	0.00	0.00	0.02	0.00	0.02	0.00	0.02	0.00	0.01	0.00	0.02
X_{usp}; X_{ilm}	0.01	0.87	0.13	0.97	0.02	0.96	0.15	0.96	0.16	0.95	0.01	1.00

Note: Total Fe measured as FeO; Fe^{3+} and mole fractions recalculated according to Stormer (1983).

in the melt. In addition, breccia xenoliths that occur in the Little Ascutney ring-dike formed by explosive eruption (Schneiderman, 1989) and are evidence of the high activity of volatile constituents in the magma. Although the syenite stock intrudes calcareous metasediments, there is no evidence for high a_{CO_2} in the magma whereas the presence of late stage amphibole and mica in the syenite suggests high a_{H_2O}.

Discussion

In its lithology, structure, and mineral chemistry, the Ascutney complex resembles other White Magma plutonic-volcanic series complexes: it consists primarily of gabbro-diorite and syenite stocks as well as biotite granite. Like other White Mountain plutonic-volcanic series complexes, Ascutney is calc-alkaline. In addition, a ring dike, so common among other members of this igneous series, occurs as part of the complex.

Behavior of the felsic constituents of the Ascutney intrusions can be modeled in the system Ab-An-Or-Q-H_2O. In the ternary subsystem Ab-An-Or (Fig. 7), bulk compositions plot in the primary phase field of plagioclase indicating that the parent liquids of the intrusions changed compositions by first crystallizing plagioclase which became increasingly sodic. Compositions of plagioclase cores and rims indicate that the liquid compositions moved toward the two feldspar boundary and would have crossed it at the reaction (odd) portion of the boundary curve. Textural evidence for this is perthite rims on plagioclase and the absence of plagioclase in micrographic intergrowths. These features indicate that plagioclase stopped crystallizing soon after alkali feldspar but before quartz appeared; that is, plagioclase ceased growing when the liquids associated with each of the intrusions passed from the plagioclase field, across the two-feldspar boundary into the primary phase field for alkali feldspar (Tuttle and Bowen, 1958).

Variations in mineral chemistry indicate crystallization histories that involved fractionation of early-formed mafic constituents and relative alkali enrichment: unzoned augite has rare orthopyroxene inclusions in the gabbro and coexists with hornblende and biotite in the diorite; zoned amphibole in the gabbro-diorite decreases in Al, Ti, and alkalis from core to rim; though uncommon, clinopyroxene occurs as inclusions in biotite and hornblende in the syenite and the granite; plagioclase is normally zoned from calcic cores to sodic rims in all intrusions. Early crystallization of orthopyroxene, augite, and calcic plagioclase depleted in the magmas in MgO and CaO while crystallization of Fe-Ti oxides depleted them in FeO and Fe_2O_3.

Isotopic data of Foland et al. (1985, 1988) indicate that the gabbro-diorite rocks of the Ascutney complex were derived by fractional crystallization of a mantle-derived basaltic magma that assimilated variable amounts of country rock. Their data indicate that the granite magma evolved, by fractional crystallization with no crustal contamination, from the mafic magma that formed the gabbro-diorite.

The major element data of this study, however, do not

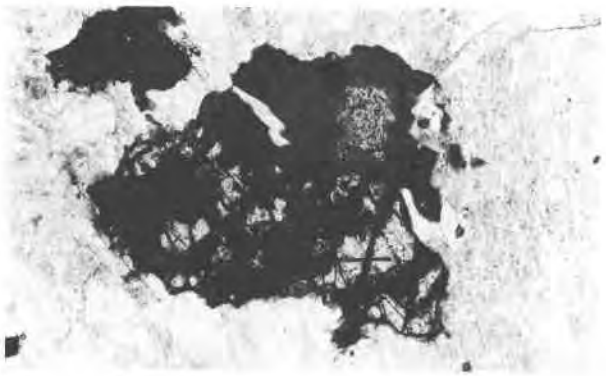

Fig. 5. Photomicrograph showing annite + quartz rimming fayalite + potassium feldspar in quartz syenite. Ascutney Mountain, Vermont, cross-polarized light (sample 5234).

unequivocally support the conclusions of Foland et al. (1985, 1988). Though the gabbro-diorite has high normative An in comparison to the granite (Fig. 7) which would suggest extensive fractional crystallization in deriving the granite from the gabbro-diorite, the Mg numbers of the hornblende in the gabbro-diorite and granite are nearly identical and imply minimal fractional crystallization.

Foland et al. (1985, 1988) did not consider the evolution or parentage of the magma which formed the syenite. Petrography and major element data from this study indicate that the syenite magma was not related to the granite magma. Feldspars in the granite have sharp grain boundaries and are unaltered, unlike those in the syenite

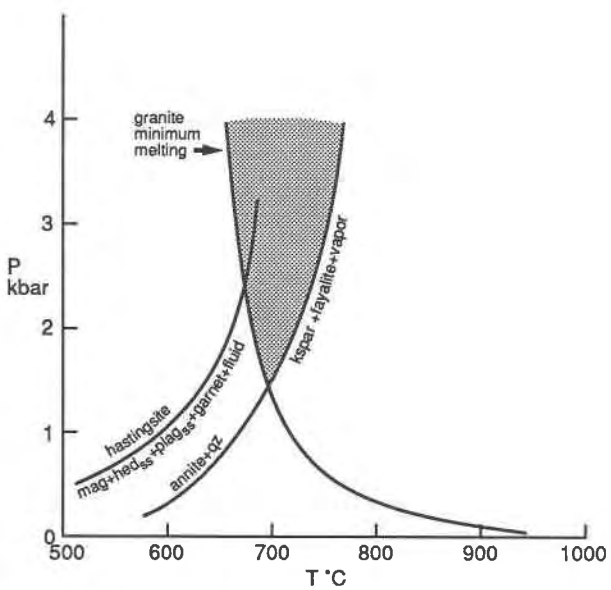

Fig. 6. Stability curves for mafic silicates in Ascutney quartz syenite (after Eugster and Wones, 1962; Thomas, 1982). Also plotted is the granite minimum melting curve (Tuttle and Bowen, 1958). Shaded area indicates *P-T* region where annite and hastingsite are stable in a granitic melt.

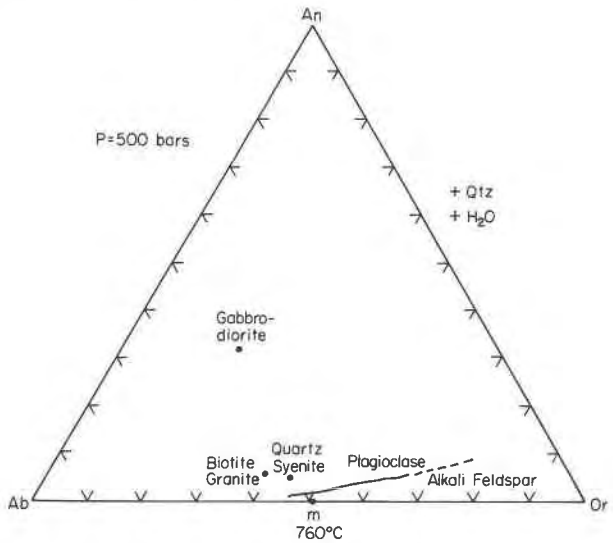

Fig. 7. Bulk compositions of gabbro-diorite and granite in terms of normative An-Ab-Or. The diagram shows the approximate liquidus surface for 500 bars. The approximate position of the quartz- and H_2O-saturated two-feldspar boundary curve is shown. Whole-rock analyses of Daly (1903) and Foland et al. (1985).

which have irregular grain boundaries and are intergrown with quartz, indicating relative H_2O enrichment. Both the amphibole and biotite in the syenite have lower Mg numbers than do those minerals in the granite. Also, amphibole in the syenite has substantial $^{[4]}$Al. In contrast, the normative proportions of An-Ab-Or and the mineral compositions in the gabbro-diorite and syenite may be consistent with a distant relation between these two parent magmas.

Summary and conclusions

Early igneous activity at Ascutney Mountain involved emplacement of radial mafic dikes and glassy felsite dikes with spherules (Balk and Krieger, 1936). Phreatomagmatic explosions occurred, perhaps as a result of the low total pressure and high a_{H_2O}, and resulted in the formation of maar-type breccias (Schneiderman, 1989). A volcanic edifice formed on the Cretaceous erosion surface, the remnants of which are preserved as a screen and inclusions in Ascutney syenite.

The three stocks and ring dike of the Ascutney complex reached crustal levels as high as the volcanic edifice itself. Intrusion of gabbro-diorite was followed by intrusion of a syenite ring dike and stock. The gabbro-diorite was cool prior to intrusion of the syenite ring dike as indicated by fine-grained porphyritic texture and chilled margins in syenite against the gabbro-diorite. The syenite stoped fragments of the surrounding country rock and intruded the volcanic structure; xenoliths of country rock and volcanics are contained in it. The last phase of igneous activity was the intrusion of biotite granite into the syenite stock.

This study shows that rocks of the Ascutney Mountain igneous complex were emplaced into Precambrian and Paleozoic country rocks at low pressure (~2 kbar) and moderate temperature (890–1000 °C) with f_{O_2} below the FMQ buffer. H_2O activity, calculated from biotite compositions in the syenite was high.

Trends in the compositions of mafic silicates and feldspars in the gabbro-diorite, syenite, and granite suggest that the magmas which formed the gabbro-diorite and granite were possibly unrelated whereas there may have been a distant relation between the gabbro-diorite and syenite magmas.

Acknowledgments

This study was supported by NSF grant EAR 8115686 to J.B. Thompson, Jr. The author thanks B.R. Frost and A. Treiman for helpful reviews. Constructive criticism by J. Longhi considerably improved the manuscript.

References cited

Albee, A.L., and Ray, L. (1970) Correction factors for electron probe microanalysis of silicates, oxides, carbonates, phosphates and sulphates. Analytical Chemistry, 42, 1408–1414.

Balk, R., and Krieger, P. (1936) Devitrified felsite dikes from Ascutney Mountain, Vermont. American Mineralogist, 21, 516–522.

Ballard, R.D., and Uchupi, E. (1975) Triassic rift structure in Gulf of Maine. American Association of Petroleum Geologists Bulletin 59, 7, 1041–1072.

Bedard, J.H. (1988) Comparative amphibole chemistry of the Monteregian and White Mountain alkaline suites, and the origin of amphibole megacrysts in alkali basalts and lamprophyres. Mineralogical Magazine, 52, 91–103.

Bence, A.E., and Albee, A.L. (1968) Empirical correction factors of the electron microanalysis of silicates and oxides. Journal of Geology, 76, 382–403.

Billings, M.P. (1928) The petrology of the North Conway quadrangle in the White Mountains of New Hampshire. Proceedings of the American Academy of Arts and Science, 63, 67–137.

——— (1943) Ring-dikes and their origin. Transactions of the New York Academy of Science Series II, 5, 131–144.

——— (1956) The geology of New Hampshire, Part II, Bedrock geology. New Hampshire State Planning and Development Commission, 203 p. Concord, New Hampshire.

Buddington, A.F., and Lindsley, D.H. (1964) Iron-titanium oxide minerals and synthetic equivalents. Journal of Petrology, 5, 310–357.

Burnham, C.W., Holloway, J.F., and Davis, N.F. (1969) Thermodynamic properties of water to 1000 °C and 10,000 bars. Geological Society of America Special Paper 132, 96 p.

Cameron, M., and Gibbs, G.V. (1973) The crystal structure and bonding of fluortremolite; a comparison with hydroxyl tremolite. American Mineralogist, 58, 879–888.

Chapman, R.W., and Chapman, C.A. (1940) Cauldron subsidence at Ascutney Mountain, Vermont. Geological Society of America Bulletin 51, 191–212.

Czmanske, G.K., and Wones, D.R. (1973) Oxidation during magmatic differentiation, Finnmarka complex, Oslo area, Norway: Part 2, the mafic silicates. Journal of Petrology, 41, 349–380.

Daly, R.A. (1903) Geology of Ascutney Mountain, Vermont. U.S. Geological Survey Bulletin 209, 122 p.

Diamond, J.L., and Frost, B.R. (1988) Mineralogical controls on rock magnetism in the Sierra San Pedro Martir pluton, Baja California, Mexico. Eos, 69, 1506.

Doll, C.G., Cady, W.M., Thompson, J.B., Jr., and Billings, M.P. (1961) Centennial geological map of Vermont. Vermont Geological Survey, Montpelier, Vermont, scale 1:250,000.

Downie, E.A. (1982) Structure and metamorphism in the Cavendish area, north end of the Chester dome, southeastern Vermont, 291 p. Ph.D thesis, Harvard University, Cambridge, Massachusetts.

Eby, G.N. (1985) Sr and Pb isotopes, U and Th chemistry of the alkaline Monteregian and White Mountain igneous provinces, eastern North America. Geochimica et Cosmochimica Acta, 49, 1143–1154.

——— (1987) The Monteregian Hills and White Mountain alkaline igneous provinces, eastern North America. In J.G. Fitton and B.G.J. Upton, Eds., Alkaline igneous rocks, p. 433–447. Blackwell, London.

Eugster, H.P., and Wones, D.R. (1962) Stability relations of the ferruginous biotite, annite. Journal of Petrology, 3, 82–125.

Fletcher, J.P., Sbar, M.L., and Sykes, L.R. (1974) Seismic zones and travel time anomalies in eastern North America related to fracture zones active in the early opening of the Atlantic. Eos, 55, 447.

Foland, K.A., and Faul, H. (1977) Ages of the White Mountain intrusives—New Hampshire, Vermont and Maine, USA. American Journal of Science, 277, 888–904.

Foland, K.A., Henderson, C.M.B., and Gleason, J. (1985) Petrogenesis of the magmatic complex at Mt. Ascutney, Vermont, USA, I: Assimilation of crust by mafic magmas based on Sr and O isotopic and major element relationships. Contributions to Mineralogy and Petrology, 90, 331–345.

Foland, K.A., Raczek, I., Henderson, C.M.B., and Hoffmann, A.W. (1988) Petrogenesis of the magmatic complex at Mt. Ascutney, Vermont, USA, II: Contamination of mafic magmas and country rock model ages based upon Nd isotopes. Contributions to Mineralogy and Petrology, 98, 408–416.

Frost, B.R., Lindsley, D.H., and Andersen, D.J. (1988) Fe-Ti oxide-silicate equilibria: Assemblages with fayalitic olivine. American Mineralogist, 73, 727–740.

Gold, D.P. (1967) Alkaline ultrabasic rocks in the Montreal area, Quebec. In P.J. Wiley, Ed., Ultramafic and related rocks, p. 288–302. Wiley, New York.

Helz, R.T. (1979) Alkali exchange between hornblende and melt: A temperature sensitive reaction. American Mineralogist, 64, 953–965.

Holdaway, M.J. (1971) Stability of andalusite and the aluminum silicate phase diagram. American Journal of Science, 271, 97–131.

Leake, B.E. (1978) Nomenclature of amphiboles. American Mineralogist, 63, 1023–1053.

McHone, J.G., and Butler, J.R. (1984) Mesozoic igneous provinces of New England and the opening of the North Atlantic Ocean. Geological Society of American Bulletin 95, 757–765.

Nielson, D.L. (1973) Silica diffusion at Ascutney Mountain, Vermont. Contributions to Mineralogy and Petrology, 40, 141–148.

Philpotts, A.R. (1974) The Monteregian province. In H. Sorenson, Ed., The alkaline rocks, p. 293–310. Wiley, New York.

Powell, M., and Powell, R. (1977) Plagioclase-alkali-feldspar geothermometry revisited. Mineralogical Magazine, 41, 253–256.

Rutherford, M.L. (1969) An experimental determination of iron biotite-alkali feldspar equilibria. Journal of Petrology, 60, 381–408.

Schneiderman, J.S. (1987) Ascutney-Mountain revisited: Petrology of the igneous complex and included breccia xenoliths, 286 p. Ph.D. thesis, Harvard University, Cambridge, Massachusetts.

——— (1989) The Ascutney Mountain breccia: Field and petrologic evidence for an overlapping relationship between New Hampshire sequence and Vermont sequence rocks. American Journal of Science, 289, 771–811.

Semet, M.O., and Ernst, W.G. (1981) Experimental stability relations of the hornblende magnesio-hastingsite. Geological Society of America Bulletin 92, 71–74.

Spencer, K.J., and Lindsley, D.L. (1981) A solution model for coexisting iron-titanium oxides. American Mineralogist, 66, 1189–1201.

Stormer, J.C. (1975) A practical two-feldspar geothermometer. American Mineralogist, 60, 667–674.

——— (1983) The effects of recalculation on estimates of temperature and oxygen fugacity from analyses of multicomponent iron-titanium oxides. American Mineralogist, 68, 586–594.

Thomas, W.M. (1977) Preliminary stability relations of the hornblende hastingsite and the effect of Fe^{3+} for aluminum replacement in amphiboles. Eos, 58, 1244.

——— (1982) Stability relations of the amphibole hastingsite. American Journal of Science, 282, 136–164.

Tuttle, O.F., and Bowen, N.L. (1958) Origin of granite in the light of experimental studies in the system $NaAlSi_3O_8$-$KAlSi_3O_8$-SiO_2-H_2O. Geological Society of America Memoir 74, 153 p.

Vink, G.E., Morgan, W.J., and Vogt, P.R. (1985) The Earth's hot spots. Scientific American, 252, 50–57.

Waldbaum, D.R., and Thompson, J.B., Jr. (1969) Mixing properties of sanidine crystalline solutions: Part IV, Phase diagrams from equations of state. American Mineralogist, 54, 1274–1298.

Wones, D.R. (1981) Mafic silicates as indicators of intensive variables in granitic magmas. Mining Geology, 31, 181–212.

Wones, D.R., and Eugster, H.P. (1965) Stability of biotite: Experiment, theory and application. American Mineralogist, 50, 1228–1272.

Manuscript received June 30, 1989
Manuscript accepted November 9, 1990